Chirality-Driven Mass Enhancement in the Kagome Hubbard Model

Masafumi Udagawa and Yukitoshi Motome

Department of Applied Physics, University of Tokyo, Tokyo 113-8656, Japan
(Received 28 December 2009; published 12 March 2010)

We investigate the quasiparticle-mass enhancement in the Hubbard model on the frustrated kagome lattice by using a cluster extension of the dynamical mean-field theory. By analyzing the cluster density matrix, we find a hierarchy of energy scale among charge, spin, and chirality degrees of freedom. A large amount of entropy associated with the chirality is released at a much lower temperature than other energy scales for spin and charge fluctuations, leading to a sharp peak in the specific heat and the single-particle spectrum. The results manifest a generic mechanism of mass enhancement driven by an emergent composite degree of freedom under geometrical frustration.

Heavy-fermion behavior is one of the most intriguing phenomena in correlated electron systems. Canonical examples are found in rare-earth compounds, in which a large quasiparticle-mass enhancement is observed, e.g., in the specific-heat coefficient γ. The origin has been argued on the basis of the Kondo effect—the screening of local f-electron moments by conduction electrons [1]. In this case, the local f-electron moments serve as an "entropy reservoir" for the heavy-mass behavior [2].

Recently, a class of transition metal compounds has drawn considerable attention due to their heavy-fermion behavior. A large γ of the order of 100 mJ/mol K^2 was observed in compounds such as LiV_2O_4 [3], $Y(Sc)Mn_2$ [4], and β-Mn [5]. The conventional Kondo scenario does not apply straightforwardly to this heavy-fermion behavior, since these $3d$-electron compounds do not have an obvious entropy reservoir like the localized f moments in the rare-earth compounds. In spite of many theoretical proposals [6–11], the issue remains controversial so far.

One of the proposals is the effect of strong electron correlation under geometrical frustration [7,9–11]. Divergence of the quasiparticle mass at the correlation-driven Mott transition was first pointed out by Brinkman and Rice [12]. Later, the dynamical mean-field theory (DMFT) provides a more sophisticated picture [13], where the electron correlation results in separation of energy scale between charge and spin (and orbital) degrees of freedom of electrons. Namely, it suppresses charge fluctuations at an energy scale of the Coulomb repulsion, and leaves large spin (and orbital) fluctuations at much lower temperatures T, which serve as an entropy reservoir [14]. This mass divergence, however, persists only when spatial correlations are neglected. Indeed, when DMFT is extended to include spatial correlations, an antiferromagnetic spin correlation develops at low T, which suppresses the local spin fluctuations and collapses the heavy-fermion state [15]. It is widely considered that this obstacle can be circumvented by the geometrical frustration: The frustration suppresses spatial correlations and rejuvenates the masked heavy-fermion behavior. Hence, in this scenario,

the heavy-fermion behavior is an intrinsic property associated with the criticality of the Mott transition, and the geometrical frustration plays a secondary role of uncovering it by suppressing spatial correlations.

In this Letter, contrary to the prevailing view, we reveal an intensive role of the geometrical frustration on the quasiparticle-mass enhancement. We show that the frustration not only suppresses the spatial correlations but also brings about a composite degree of freedom, and it plays a role of the entropy reservoir. It is known that composite objects, such as spin chirality [16] and self-organized clusters [17–19], often emerge in insulating systems, but we here explore the importance of such composites in correlated metals. Through the study of the kagome-lattice Hubbard model, we demonstrate that the spin chirality degree of freedom emerges and plays a dominant role in the mass enhancement.

We consider the Hubbard model on the kagome lattice shown in Fig. 1(a),

$$\mathcal{H} = -t \sum_{\langle ij \rangle, \sigma} (c_{i\sigma}^\dagger c_{j\sigma} + \text{H.c.}) + U \sum_i n_{i\uparrow} n_{i\downarrow}, \qquad (1)$$

where the sum of $\langle ij \rangle$ is taken over the nearest-neighbor sites and $n_{i\sigma} = c_{i\sigma}^\dagger c_{i\sigma}$. The model has been extensively studied as a minimal model with electron correlation and
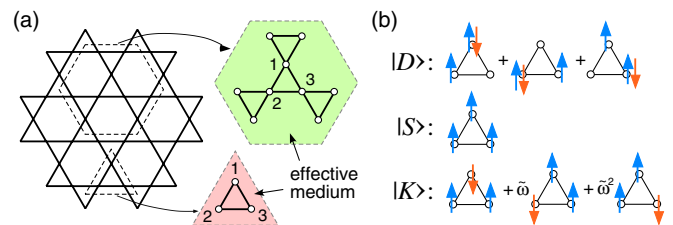

FIG. 1 (color online).   (a) Schematic picture of the mapping of the kagome lattice to three and nine-sites clusters in the CDMFT calculations. The three-site density matrix is calculated for the numbered three sites in each cluster. (b) Schematic pictures of the doublon, spin-polarized, and chiral states defined in Eqs. (3)–(5).

geometrical frustration [20–23]. We set $t = k_B = \hbar = 1$, and fix the electron density at half filling.

We adopt the cellular dynamical mean-field theory (CDMFT) [24] to study this model, which is an extension of DMFT to include the effect of spatial correlations within a cluster. The method is basically the same as that used in Ref. [22]; however, in the present study, we perform the CDMFT calculations for two different clusters with three and nine sites (Fig. 1) to check the cluster-size dependence. Moreover, as a solver for the effective cluster model, we employ the continuous-time auxiliary-field quantum Monte Carlo (MC) method based on the perturbation expansion in terms of U [25]. This solver gives precise results more efficiently compared with the conventional Hirsch-Fye algorithm used in Ref. [22]. Typically we take 256 imaginary-time slices and 10^6 MC steps, and the convergence is reached after 20 self-consistency loops, e.g., at $U = 6$ and $T = 0.1$. Larger computational cost is required at lower T and larger U, in particular, in the calculations of the specific heat and the entropy (see below).

In order to identify the relevant degrees of freedom in the system, we calculate the cluster density matrix, which gives the probability distribution of quantum mechanical states within the cluster. Here we consider the density matrix defined on the three sites within each cluster indicated in Fig. 1. We calculate the diagonal components

$$\rho_\Psi = \frac{1}{Z} \text{Tr}(|\Psi\rangle\langle\Psi| e^{-\mathcal{H}/T}) \tag{2}$$

for a cluster state $|\Psi\rangle$, where Z is the partition function. The $4^3 = 64$ states are classified by irreducible representations under the $U(1) \otimes SU(2) \otimes C_{3v}$ symmetry of the model. Among them, we focus on ρ_Ψ for the following three states (and their symmetrically equivalent ones):

$$|D\rangle = \frac{1}{\sqrt{3}}(|\uparrow\downarrow, \uparrow, 0\rangle + |0, \uparrow\downarrow, \uparrow\rangle + |\uparrow, 0, \uparrow\downarrow\rangle), \tag{3}$$

$$|S\rangle = |\uparrow, \uparrow, \uparrow\rangle, \tag{4}$$

$$|K\rangle = \frac{1}{\sqrt{3}}(|\downarrow, \uparrow, \uparrow\rangle + \tilde{\omega}|\uparrow, \downarrow, \uparrow\rangle + \tilde{\omega}^2|\uparrow, \uparrow, \downarrow\rangle), \tag{5}$$

where $|\uparrow\downarrow, \uparrow, 0\rangle \equiv c_{1\uparrow}^\dagger c_{1\downarrow}^\dagger c_{2\uparrow}^\dagger|\text{vac}\rangle$, etc., ($|\text{vac}\rangle$ is a vacuum), and $\tilde{\omega}$ is a phase factor defined below. Here, we call $|D\rangle$ the doublon state which includes a doublon-holon pair, $|S\rangle$ the spin-polarized state with the total spin $S = 3/2$, and $|K\rangle$ the chiral state. Among these states, the chiral state is of special interest. $|K\rangle$ retains fourfold degeneracy with its time-reversal and reflection conjugate states: The four states are labeled by the two discrete quantum numbers, the z component of total spin $S_z^{\text{tot}} = \pm 1/2$ and the helicity $\eta = \pm 1$ [$\tilde{\omega}$ in Eq. (5) is given by $\exp(i\frac{2}{3}\pi\eta)$]. We note that the chiral states are the eigenstates of scalar- and vector-chirality operators, studied in the previous CDMFT study [26].

Figure 2 shows our CDMFT results for the density matrices, ρ_D, ρ_S, and ρ_K, in the correlated metallic region at $U = 6$. (The critical value for the Mott transition was
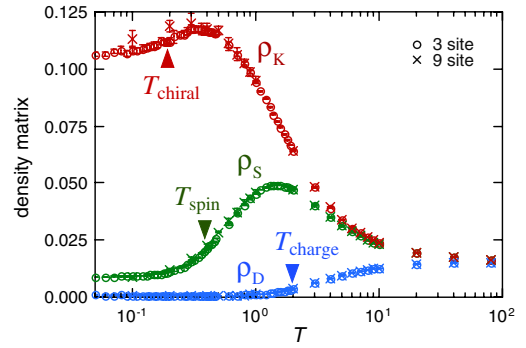

FIG. 2 (color online). Temperature dependences of the three-site density matrices, ρ_D, ρ_S, and ρ_K. The results for the three (nine)-site cluster are shown by circles (crosses).

estimated at $U_c \simeq 8.2$ [22].) The three components show qualitatively different T dependences. At high enough T, $\rho_D \approx \rho_S \approx \rho_K \approx 1/64$, since all the 64 states have nearly equal weights. While lowering T, ρ_D is suppressed but ρ_S and ρ_K are enhanced. ρ_S turns to decrease with showing a broad peak at $T \sim 1.2$. ρ_K continues to increase down to lower T, but finally turns to decrease with showing a peak at $T \sim 0.32$. It is noteworthy that the results show little cluster-size dependence as shown in Fig. 2: This indicates that our CDMFT results show good convergence to the thermodynamic limit. Such rapid convergence may be attributed to suppressed intertriangular correlations under the corner-sharing topology of the kagome lattice, as discussed in the localized spin models [27,28].

These characteristic T dependences indicate a hierarchy of energy scale for relevant degrees of freedom. Charge fluctuations are first suppressed by large U, being signaled by the suppression of ρ_D which includes a doublon-holon pair. At a lower energy scale where ρ_S decreases steeply, the spin degree of freedom is frozen out, and finally, the chirality is quenched at the lowest energy scale, corresponding to the suppression of ρ_K. We identify the characteristic energy scales for charge, spin, and chirality degrees of freedom by the temperatures T_{charge}, T_{spin}, and T_{chiral} where ρ_D, ρ_S, and ρ_K are suppressed most rapidly (Fig. 2). The hierarchy is clearly seen as $T_{\text{charge}} \simeq 2.0 > T_{\text{spin}} \simeq 0.37 > T_{\text{chiral}} \simeq 0.18$.

We investigate the energy hierarchy systematically in the correlated metallic region. Figures 3(a)–3(c) show T dependences of ρ_D, ρ_S, and ρ_K with varying U. The estimated characteristic temperatures are summarized in the crossover phase diagram in Fig. 3(d). T_{charge} increases as U increases, which is reasonable since charge fluctuations are suppressed below $T \simeq U - W^*$ (W^* is a renormalized band width). On the other hand, T_{spin} decreases as U increases. We compare T_{spin} with an effective super-exchange interaction $J = 4t^2/U$, derived in the strong-coupling expansion in t/U, and find approximately $T_{\text{spin}} \approx J/2$. This suggests that the reduction of ρ_S is a strong-correlation effect, originating from the effective spin exchange under suppressed charge fluctuations. T_{chiral} also
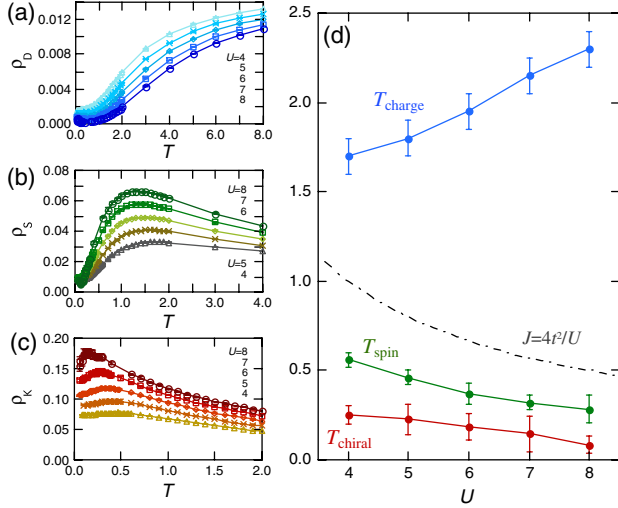
FIG. 3 (color online).   Temperature dependences of the density matrices (a) ρ_D, (b) ρ_S, and (c) ρ_K. The results are for the three-site cluster and the lines are guides for the eye. The characteristic energy scales T_{charge}, T_{spin}, and T_{chiral}, determined by the steep decrease of ρ_D, ρ_S, and ρ_K, are plotted as a function of U in (d). The dashed line shows the effective exchange interaction $J = 4t^2/U$ for comparison.

decreases as U increases, and is always located well below T_{spin}. This indicates that the composite chiral degree of freedom is dominated by a much smaller energy scale compared with J.

The energy hierarchy and the quenching of each degree of freedom are also observed from the entropic point of view. Figures 4(a) and 4(b) show the CDMFT results for the specific heat C and the entropy S, respectively. Here, we calculated C by numerical differentiation of the internal energy: To obtain the high precision data, we took a large number of imaginary-time slices, e.g., 8192 slices at $T \simeq 0.1$ and $U \simeq 6$ [29]. The entropy S is obtained by the numerical integration of C/T. As a result, C shows a sharp peak at low $T \simeq T_{\text{chiral}}$ in addition to a broad peak at $T \sim T_{\text{charge}}$. The broad peak comes from the release of charge entropy; the peak temperature shifts to higher in accord with T_{charge} while increasing U (not shown). On the other hand, the low-T sharp peak originates from the entropy release associated with the chirality: In fact, as shown in Fig. 4(b), the entropy S takes a value close to $\log 4/3$ at T_{chiral}, corresponding to the fourfold degeneracy of the chiral states $|K\rangle$. It is difficult to see a clear structure in C at $T \simeq T_{\text{spin}}$; however, S reaches nearly $\log 8/3$ at T_{spin}, reflecting the fourfold spin-polarized states $|S\rangle$ in addition to the four chiral states. Our results indicate that the entropy associated with chirality, spin, and charge degrees of freedom is released at separated energy scales T_{chiral}, T_{spin}, and T_{charge} in Fig. 3(d). To our knowledge, the resultant sharp peak in the specific heat due to the chirality has never been found in the previous studies.

The sharp peak is considered a hallmark of the formation of Fermi liquid state below T_{chiral}. In fact, as shown in
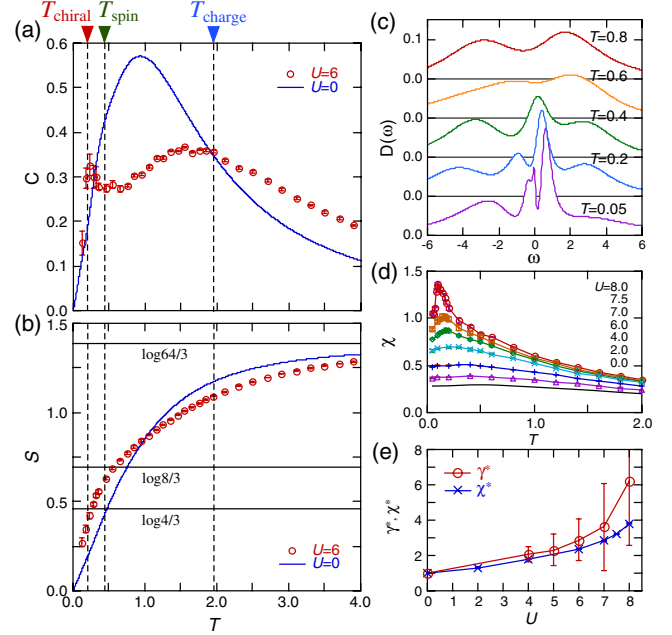

FIG. 4 (color online).   Temperature dependences of (a) specific heat and (b) entropy at $U = 6$ per site. The results at $U = 0$ are shown for comparison. Three vertical dashed lines indicate the characteristic temperatures estimated in Fig. 3, and three horizontal lines in (b) show the values of $\log 4/3$, $\log 8/3$, and $\log 64/3$. (c) Single-particle spectrum at $U = 6$ obtained by the maximum entropy method. (d) Temperature dependence of the uniform magnetic susceptibility. (e) Enhancement factors of the specific-heat coefficient estimated from T_{chiral}, γ^*, and of the uniform magnetic susceptibility at $T = 0.05$, χ^*. See the text for details. All the results are obtained by the three-site cluster DMFT.

Fig. 4(c), the single-particle spectrum develops a sharp coherence peak at the Fermi level $\omega = 0$ below T_{chiral}. In addition, as plotted in Fig. 4(d), the uniform magnetic susceptibility χ approaches a nonzero value as $T \to 0$ after showing a broad peak at around T_{chiral}. All the results consistently indicate that a Fermi liquid state emerges at low T and the effective Fermi temperature is set by T_{chiral}.

In the low-T Fermi liquid state, the quasiparticle mass is largely enhanced because the effective Fermi temperature T_{chiral} is suppressed. Although it is difficult to estimate the specific-heat coefficient γ directly from the low-T data of C, we obtain a rough estimate of γ from the value of T_{chiral}: Assuming that the chiral entropy $\log 4/3$ is released uniformly in the range of $0 < T < T_{\text{chiral}}$, we obtain the mass enhancement factor $\gamma^* = \gamma/\gamma_0 \simeq \log 4/(3 T_{\text{chiral}} \gamma_0) \simeq 3$ at $U = 6$, where $\gamma_0 \simeq 0.873$ is the specific-heat coefficient at $U = 0$. As T_{chiral} is suppressed for larger U [Fig. 3(d)], γ^* is enhanced with increasing U, as shown in Fig. 4(e). We also plot the enhancement factor $\chi^* = \chi/\chi_0$ estimated at $T = 0.05$, where χ_0 is the susceptibility at $U = 0$. The results of γ^* and χ^* consistently indicate a chirality-driven mass enhancement near the Mott transition.

In the formation of the heavy-quasiparticle state, the geometrical frustration plays an essential role, not only to

suppress antiferromagnetic correlations but to bring about the degeneracy due to high local symmetry—in the present model, the fourfold degeneracy of the chiral states in the triangular unit. In general, geometrically-frustrated lattices possess such a local unit with high symmetry, e.g., triangles or tetrahedra, and hence, it is commonly expected that similar locally-degenerate state emerges. Our finding provides a prototypical example for the ubiquitous phenomenon in frustrated systems under strong correlation, that is, crossover from highly-symmetric local states to Fermi liquid state with an enhancement of quasiparticle mass. We believe that the local degeneracy and emergent composite degree of freedom are of primary importance for the puzzling heavy-fermion state in transition metal compounds, such as LiV_2O_4 [3], Y(Sc)Mn$_2$ [4], and β-Mn [5].

Finally let us remark on the fate of T_{chiral} as the system enters the Mott insulating region at larger U. In the sense that it sets the effective Fermi temperature, T_{chiral} might terminate at the first-order Mott phase boundary. We note in fact that T_{chiral} in Fig. 3(d) appears to approach the critical point (U_c, T_c) suggested in Ref. [22]. On the other hand, the spin chirality itself can be important even in the insulating region: Higher-order perturbations in terms of t/U give higher-order exchange interactions in the effective spin model, which may induce composite spin objects, such as the chirality. Unfortunately it is hard to clarify how T_{chiral} behaves at $U > 8$ because of the limitation of our simulation, and some complementary study is highly desired. An interesting issue related to this problem is the recent experimental observation of a sharp peak in the low-T specific heat of ^{3}He on graphite at a commensurate filling 4/7 [30]. It has been argued that the system is insulating but in the vicinity of the Mott transition [31], and the geometry of ^{3}He atoms has frustration in between triangular and kagome lattices [32].

In summary, we have studied the correlated metallic region of the Hubbard model on the kagome lattice by the cellular dynamical mean-field theory, with the continuous-time auxiliary-field quantum Monte Carlo method as an impurity solver. We found that, in addition to charge and spin, the chirality degree of freedom becomes relevant in this system, and energy hierarchy appears among charge, spin, and chirality. Moreover, we showed that the quasiparticle state with strongly renormalized mass is stabilized at low temperatures, as a manifestation of the strong frustration. The heavy-quasiparticle state is formed by the entropy release associated with the emergent composite degree of freedom, the chirality. This chirality-driven mass enhancement provides a prototypical example for the large mass behavior in frustrated systems under strong correlation, and gives a clue to controversies on the heavy-fermion behavior of transition metal compounds such as LiV_2O_4. It is interesting to extend the study for more realistic models by considering the effect of carrier doping and orbital degrees of freedom.

[1] J. Kondo, Prog. Theor. Phys. **32**, 37 (1964).
[2] A. C. Hewson, *The Kondo Problem to Heavy Fermions* (Cambridge Univ. Press, Cambridge, 1993), and references therein.
[3] S. Kondo *et al.*, Phys. Rev. Lett. **78**, 3729 (1997).
[4] H. Wada *et al.*, J. Magn. Magn. Mater. **70**, 17 (1987).
[5] T. Shinkoda, K. Kumagai, and K. Asayama, J. Phys. Soc. Jpn. **46**, 1754 (1979).
[6] V. I. Anisimov *et al.*, Phys. Rev. Lett. **83**, 364 (1999).
[7] V. Eyert *et al.*, Europhys. Lett. **46**, 762 (1999).
[8] H. Kusunose, S. Yotsuhashi, and K. Miyake, Phys. Rev. B **62**, 4403 (2000).
[9] H. Tsunetsugu, J. Phys. Soc. Jpn. **71**, 1844 (2002).
[10] Y. Yamashita and K. Ueda, Phys. Rev. B **67**, 195107 (2003).
[11] K. Hattori and H. Tsunetsugu, Phys. Rev. B **79**, 035115 (2009).
[12] W. F. Brinkman and T. M. Rice, Phys. Rev. B **2**, 4302 (1970).
[13] A. Georges *et al.*, Rev. Mod. Phys. **68**, 13 (1996).
[14] A. Georges and W. Krauth, Phys. Rev. B **48**, 7167 (1993).
[15] Y. Z. Zhang and M. Imada, Phys. Rev. B **76**, 045108 (2007).
[16] S. Miyashita and H. Shiba, J. Phys. Soc. Jpn. **53**, 1145 (1984).
[17] P. G. Radaelli *et al.*, Nature (London) **416**, 155 (2002).
[18] S.-H. Lee *et al.*, Nature (London) **418**, 856 (2002).
[19] Y. Horibe *et al.*, Phys. Rev. Lett. **96**, 086406 (2006).
[20] Y. Imai, N. Kawakami, and H. Tsunetsugu, Phys. Rev. B **68**, 195103 (2003).
[21] N. Bulut, W. Koshibae, and S. Maekawa, Phys. Rev. Lett. **95**, 037001 (2005).
[22] T. Ohashi, N. Kawakami, and H. Tsunetsugu, Phys. Rev. Lett. **97**, 066401 (2006).
[23] B. H. Bernhard, B. Canals, and C. Lacroix, J. Phys. Condens. Matter **19**, 145258 (2007).
[24] G. Kotliar *et al.*, Phys. Rev. Lett. **87**, 186401 (2001).
[25] E. Gull *et al.*, Europhys. Lett. **82**, 57003 (2008).
[26] M. Udagawa and Y. Motome, J. Phys. Conf. Ser. **200**, 012214 (2010).
[27] P. Leung and V. Elser, Phys. Rev. B **47**, 5459 (1993).
[28] R. Moessner and J. T. Chalker, Phys. Rev. B **58**, 12049 (1998).
[29] Our results look different from the previous ones in T. Ohashi *et al.*, J. Magn. Magn. Mater. **310**, 879 (2007), presumably because of the improved precision by the continuous-time QMC.
[30] K. Ishida *et al.*, Phys. Rev. Lett. **79**, 3451 (1997).
[31] S. Watanabe and M. Imada, J. Phys. Soc. Jpn. **76**, 113603 (2007).
[32] T. Koretsune, M. Udagawa, and M. Ogata, Phys. Rev. B **80**, 075408 (2009).